Preparation, characterization and luminescence properties of perovskite $La_2Ti_2O_7:Eu^{3+}$ nanobelts by electrospinning

FEI BI[1,*], RENYUAN LIU[2], GUANGQING GAI[1,*], XIANGTING DONG[2,*]
[1]*Laboratory of Building Energy-Saving Technology Engineering, College of Material Science and Engineering, Jilin Jianzhu University, Changchun 130118, China*
[2]*Key Laboratory of Applied Chemistry and Nanotechnology at Universities of Jilin Province, Changchun University of Science and Technology, Changchun 130022, China*

Quasi-one-dimensional $[La(NO_3)_3+Eu(NO_3)_3+Ti(SO_4)_2]$/PVP composite nanobelts were fabricated via electrospinning, and $La_2Ti_2O_7:Eu^{3+}$ nanobelts have been obtained after the relevant composite nanobelts were calcined at 800 ºC in air for 8h. The structural properties were characterized by x-ray diffraction(XRD), field emission scanning electron microscope(FESEM), and transmission electron microscope(TEM). XRD analysis indicates that $La_2Ti_2O_7:Eu^{3+}$ nanobelts are monoclinic in structure with space group $P2_1$. FESEM and TEM analysis indicate the surface of $[La(NO_3)_3+Eu(NO_3)_3+Ti(SO_4)_2]$/PVP composite nanobelts is smooth, the width is *ca.* 3-4 μm, and the thickness is *ca.* 160 nm. $La_2Ti_2O_7:Eu^{3+}$ nanobelts are composed of nanorods with the length ranging from 270 to 660 nm. The width of $La_2Ti_2O_7:Eu^{3+}$ nanobelts is *ca.* 3 μm, and the thickness is *ca.* 140 nm. The photoluminescent(PL) properties of the $La_2Ti_2O_7:Eu^{3+}$ nanobelts were also studied. It is observed that the charge-transfer excitation bands of Eu^{3+} in the nanobelts are red-shifted with the increase of doping Eu^{3+} ion concentration. Under ultraviolet excitation of 274 nm, the $La_2Ti_2O_7:Eu^{3+}$ nanobelts emit the main emission peak at 615 nm, corresponding to $^5D_0 \rightarrow {}^7F_2$ transition of Eu^{3+}. The PL emission intensity of Eu^{3+} increases with its doping concentration from 1 mol% to 9 mol% without concentration quenching effect. Possible formation mechanism of $La_2Ti_2O_7:Eu^{3+}$ nanobelts was proposed.

(Received October 25, 2022; accepted April 5, 2023)

Keywords: Electrospinning, $La_2Ti_2O_7$, Nanobelt, Luminescence properties

1. Introduction

One-dimensional(1D) and Quasi-one-dimensional(Q-1D) nanostructures, such as nanowires, nanofibers, nanorods, nanobelts, and nanotubes, have attracted great research interests due to their potentials in fundamental studies and technological applications [1-7]. Up to now, various techniques have been explored to prepare 1D and Q-1D nanomaterials, such as laser ablation, vapor-phase approach, template, and other methods [8-10].

Layered compounds have been regarded as attractive functional materials that serve two-dimensional microspaces, (110)-layered perovskite Lanthanum titanate ($La_2Ti_2O_7$) has attracted widespread attention owing to its excellent dielectric, electrical, mechanical and luminescence properties [11-16]. The $La_2Ti_2O_7$ nanomaterials have been widely used in the fields of piezoelectric ceramics, light-emitting devices and electrochemical energy storage. Large dielectric constant, low dielectric loss and high Curie temperature make $La_2Ti_2O_7$ an excellent piezoelectric ceramic material. The $La_2Ti_2O_7$ has a low phonon energy (806 cm^{-1}) and a wide band gap, which can serve as the substrate material [17] for the rare-earth light-emitting center. Jin et al. synthesized the $La_2Ti_2O_7$: Eu^{3+} fluorescent material by solvent heat method, which emits strong red light under ultraviolet light (254 nm), clearly displaying the fingerprint details [18] on various materials. Erdem et al. prepared a series of Yb^{3+}/Er^{3+} co-doped $La_2Ti_2O_7$ phosphors by the solid-phase method, and found that they can achieve wide-band white light emission at higher pump power and have a sensitivity of [19] with low optical thermometry.

Electrospinning technology has been extensively explored as a simple and versatile method for forming inorganic superfine nanofibers using polymer/inorganic composite as the precursor [20-22]. The morphology of materials can be controlled by adjusting experimental conditions, such as the viscosity of spinning solution, relative air humidity, the structure of spinneret, spinning voltage, and the distance between the spinneret and the collector. Advantages of this novel process for fabricating 1D nanostructures include, but is not limited to, low cost, high efficiency and convenient assembly. It has been reported that the nanofibers was successfully synthesized *via* electrospinning [23, 24].

In this paper, we report the preparation of Eu^{3+}doped $La_2Ti_2O_7$ nanobelts phosphors via a simple and effective electrospinning method. We also investigate the structure, morphology, and PL properties of the resulting samples in detail and some meaningful results were obtained.

2. Experimental sections

2.1. Chemicals

Polyvinylpyrrolidone(PVP, K-90) and N,N-dimethylformamide(DMF) were purchased from Tianjin Tiantai Fine Chemical Reagents Co., Ltd. and HNO_3(A.R.) was bought from Beijing Chemical Company. Eu_2O_3, $La(NO_3)_3 \cdot 6H_2O$ and $Ti(SO_4)_2$ were bought from Sinopharm Chemical Reagents Co. Ltd. $Eu(NO_3)_3$ was prepared by dissolving Eu_2O_3 in dilute nitric acid, then evaporated the water from the solution by heating. 40 wt% $Ti(SO_4)_2$ was prepared by dissolving $Ti(SO_4)_2$ into deionized water. All chemicals were of analytical grade and directly used as received without further purification.

2.2. Preparation of samples

$La_2Ti_2O_7$:x mol%Eu^{3+}(x=0,1,5,7,9) were prepared by a method of electronspinning combined with sol–gel process. In a typical procedure of preparing $La_2Ti_2O_7$:5 mol%Eu^{3+}, 0.95 mmol $La(NO_3)_3 \cdot 6H_2O$, 0.05 mmol $Eu(NO_3)_3$ and 0.6 g 40 wt% $Ti(SO_4)_2$ were dissolved in 9.0 g DMF, a certain amount of PVP(16 wt%) was added. The precursor sol was stirred for 8 h to form a homogeneous mixture sol for further electrospinning.

The schematic diagram of the electrospinning setup is shown in Fig. 1. It consists of three major components: a high voltage power supply, a spinneret(syringe), and a collector plate(a grounded conductor). The precursor sol was loaded into the syringe. In a typical electrospinning process, the precursor sol was ejected from the tip of the spinneret under the effect of high voltage that was applied between the spinneret and the collector to form an electrically charged jet of sol. The sol jet solidified along with evaporation of solvent and formed a nonwoven mat on the collector [1].

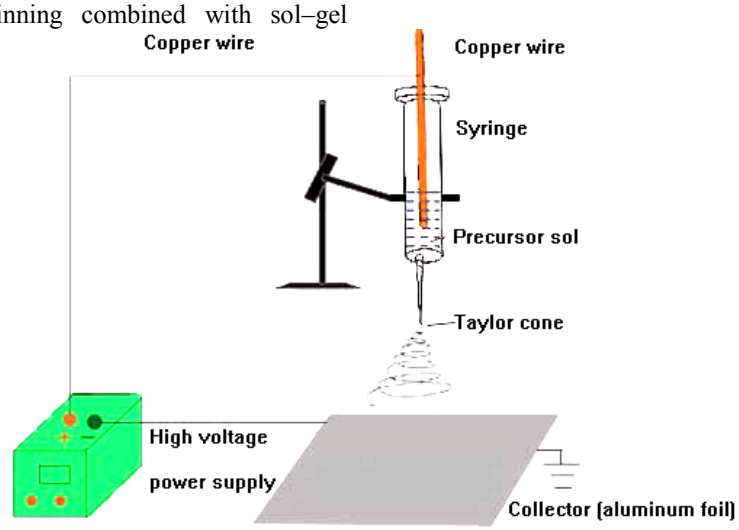

Fig. 1. Schematic diagram of the electrospinning setup (color online)

The distance between the spinneret(a plastic needle) and collector(aluminum foil) was fixed at 20 cm and the high voltage supply was maintained at 10 kV. The room temperature is 20-24 °C and the relative humidity is 50-60 %. $[La(NO_3)_3+Ti(SO_4)_2+Eu(NO_3)_3]$/PVP composite nanofibers would be fabricated. $La_2Ti_2O_7$:5 mol% Eu^{3+} nanobelts can be obtained when the relevant composite nanobelts were annealed in air at the desired temperature for 10h with the heating rate of 1 °C·min^{-1}. Other series of $La_2Ti_2O_7$:x mol%Eu^{3+}(x=0-9) were prepared by the similar procedure except for different ratios of rare earth salts in sol.

2.3. Characterization methods

X-ray powder diffraction(XRD) measurements were carried out on a Dandong Y-2000 diffractometer using Cu Ka radiation with Ni filter(λ=0.15405 nm). Thermogravimetric and differential thermal analysis(TG-DTA) data were recorded with Pyris Diamond TG-DTA(Perkin Elmer Thermal Analyzer) with the heating rate of 10 ℃ min^{-1} in an air flow of 25 ml·min^{-1}. Morphology and composition of the samples were analyzed using a field emission scanning electron microscope(FESEM, XL-30, FEI Company). Transmission electron microscopy(TEM) analysis was carried out using a JEM-2010 transmission electron microscope under a working voltage of 200 kV. The photoluminescence(PL) measurements were performed on a Hitachi F-7000 spectrophotometer equipped with a 150W xenon lamp as the excitation source.

3. Results and discussion

3.1. TG-DTA analysis

Fig. 2 shows the thermal behavior of $[La(NO_3)_3+Ti(SO_4)_2)]$/PVP composite nanobelts. The weight loss was involved in four stages in TG curve. The first weight loss is 9 % in the range of 40 to 160 ℃ accompanied by a small endothermic peak near 77 ℃ in the DTA curve, which is caused by the loss of the surface absorbed water or the solvents DMF in the composite

nanobelts. The second weight loss(46 %) is between 160 and 350 ºC accompanied by a sharp exothermic peaks near 330 °C in the DTA curve because of the decomposition of the nitrate and PVP.[16] The third weight loss is 22 % in the temperature ranged from 350 to 500 ºC. In the DTA curve a small exothermic peak is located at 446 ºC, which attribute to the oxidation of carbon and carbon monoxide released by the decomposition of PVP.[8] The fourth weight loss(10 %) accompanied by a small exothermic peak near 540 ºC in the DTA curve is the result of the decomposition of titanium sulfate and residual organics. And above 800 °C, the TG and DTA curves are all stable, indicating that solvents, organic compounds, nitrate and titanium sulfate in the composite nanobelts decompose and volatilize completely and pure $La_2Ti_2O_7$ is obtained after 800 ºC. The total weight loss is 87 %.

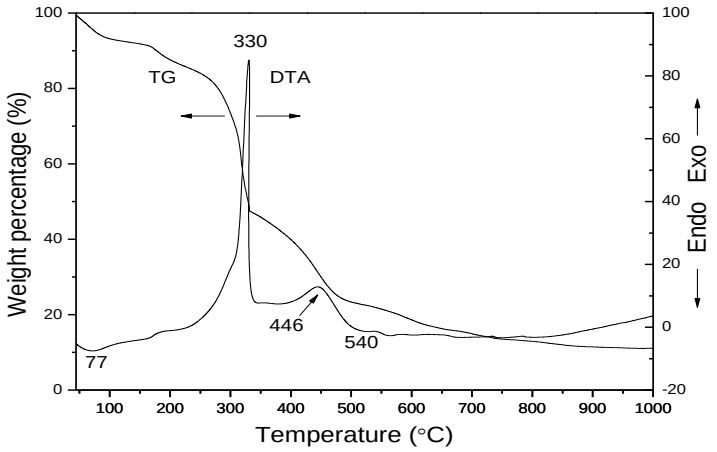

Fig. 2. TG-DTA curves of the [La(NO₃)₃+Ti(SO₄)₂]/PVP composite nanobelts

3.2. XRD analysis

The composition and phase purity of the products were examined by XRD, as shown in Fig. 3. From Fig. 3 (a), no diffraction peaks are observed, indicating that the $[La(NO_3)_3+Ti(SO_4)_2]$/PVP composite nanobelts are amorphous in structure, $La_2Ti_2O_7$ annealed at 700 °C are also amorphous, as shown in Fig. 3 (b). For the $La_2Ti_2O_7$ annealed at 800 °C shown in Fig. 3 (c), well-defined diffraction peaks can be readily indexed to those of the monoclinic phase of $La_2Ti_2O_7$(PDF 28-0517) with space group $P2_1$ according to the PDF standard card(No.28-0517) of $La_2Ti_2O_7$.

For the Eu^{3+}doped $La_2Ti_2O_7$ calcined at 800 °C, crystalline $La_2Ti_2O_7$ can be seen from Fig. 4, and all of the diffraction peaks can be readily indexed to those of pure monoclinic phase with primitive structure of $La_2Ti_2O_7$(PDF 28-0517). No second phase is detected at these doping levels, indicating that the Eu^{3+} ions can be efficiently built into the $La_2Ti_2O_7$ host lattice by replacing of the La^{3+} ion. The diffraction peaks of $La_2Ti_2O_7$:Eu^{3+} samples are shifted a little to higher angles compared with the peaks position of standard $La_2Ti_2O_7$ patterns. This is because Eu^{3+} is smaller than La^{3+} in the $La_2Ti_2O_7$ host lattice(radius(La^{3+})=0.1061 nm, radius(Eu^{3+})=0.0950 nm). However, the shift is very small due to the low doping concentration of Eu^{3+}.

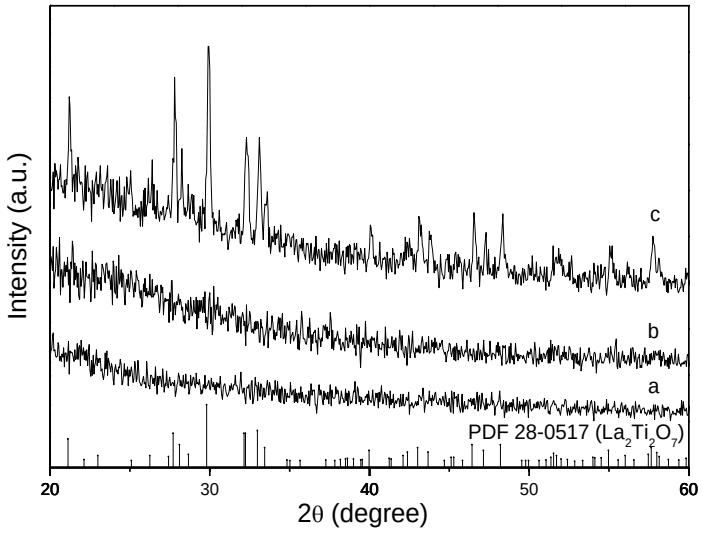

Fig. 3. XRD patterns of [La(NO₃)₃+Ti(SO₄)₂]/PVP composite nanobetlts(a) and La₂Ti₂O₇ annealed at 700 °C(b), 800 °C (c) for 10 h with the PDF standard card of La₂Ti₂O₇

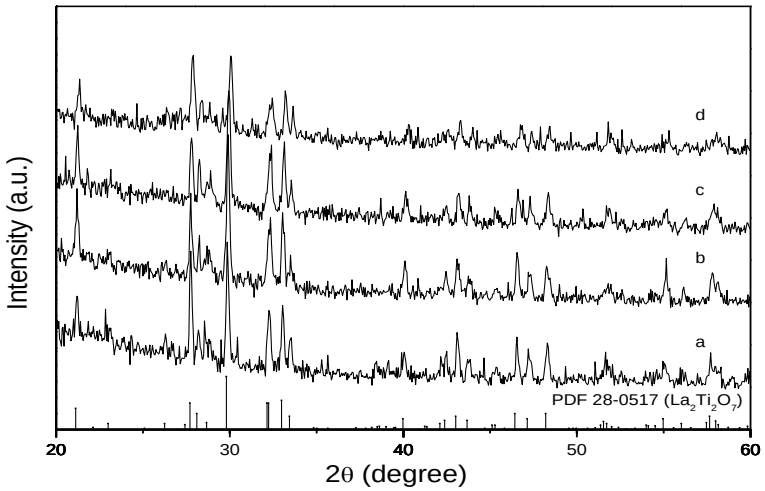

Fig. 4. XRD patterns of $La_2Ti_2O_7$:x mol%Eu^{3+}[x=1(a),5(b),7(c),9(d)] annealed at 800 °C for 10 h with the PDF standard card of $La_2Ti_2O_7$

3.3. SEM and TEM analysis

Fig. 5 shows the representative SEM images and the width distribution histograms of the $[La(NO_3)_3+Ti(SO_4)_2)+Eu(NO_3)_3]$/PVP composite nanobelts and $La_2Ti_2O_7$:5 % Eu^{3+} nanobelts annealed at 800 °C for 10 h. From the SEM image of Fig. 5 (a) and Fig. 5(b), it can be noticed that he $[La(NO_3)_3+Ti(SO_4)_2)+Eu(NO_3)_3]$/PVP composite nanobelts have smooth surface with good dispersivity. Fig. 5(c) and Fig. 5 (d) reveal that $La_2Ti_2O_7$:5%Eu^{3+} nanobelts retain their 1D morphology.

The histograms of width distribution of samples are measured by randomly selecting 100 nanobelts, as revealed in Fig. 5e and Fig. 5f. Under the 95 % confidence level, the width distribution histograms of the $[La(NO_3)_3+Ti(SO_4)_2)+Eu(NO_3)_3]$/PVP composite nanobelts and $La_2Ti_2O_7$:5 % Eu^{3+} nanobelts analyzed by Shapiro-Wilk method are normal distribution. Distribution histograms of width of the samples are indicated in Fig. 5(e) and Fig. 5(f). The width of $[La(NO_3)_3+Ti(SO_4)_2)+Eu(NO_3)_3]$/PVP composite nanobelts and $La_2Ti_2O_7$:5 % Eu^{3+} nanobelts are *ca.* 4.5 μm, and *ca.* 3μm, respectively.

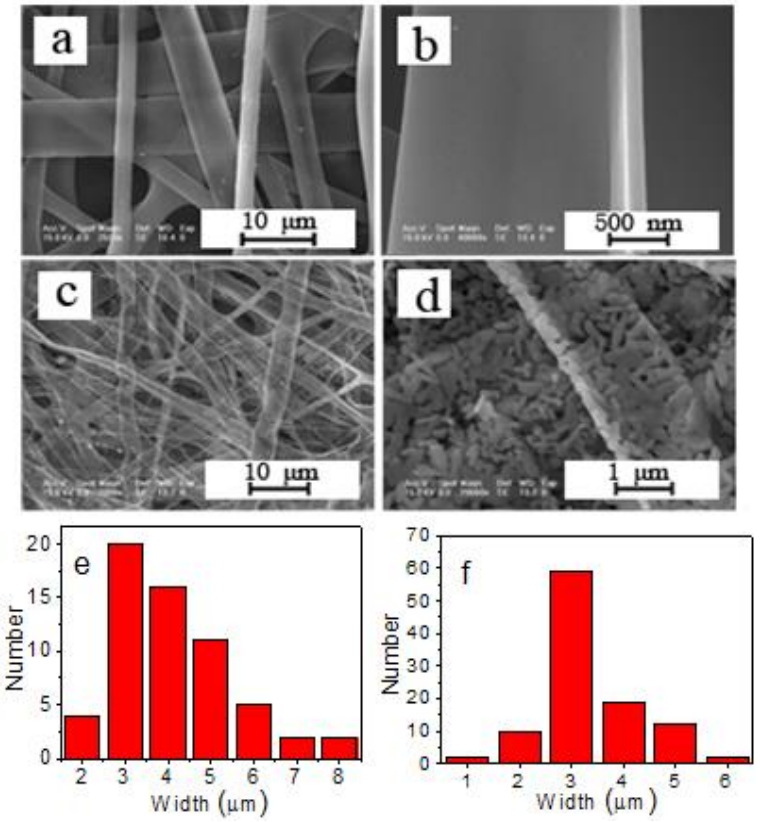

Fig. 5. SEM images and the width distribution histograms of the $[La(NO_3)_3+Ti(SO_4)_2)+Eu(NO_3)_3]$/PVP composite nanobelts(a, b, e) and $La_2Ti_2O_7$:5 % Eu^{3+} nanobelts annealed at 800 °C for 10 h(c, d, f) (color online)

TEM images of the $La_2Ti_2O_7$:5%Eu^{3+} nanobelts are illustrated in Fig. 6 (a) and Fig. 6 (b). The porous nanobelts are formed. The nanobelts consist of linked nanorods. The results are well consistent with the results of SEM analysis. The SAED patterns in Fig. 6 (c) exhibit a typical single crystalline diffraction pattern of $La_2Ti_2O_7$ phase, which also indicate that the $La_2Ti_2O_7$:5%Eu^{3+} crystallites are well crystallized [15].

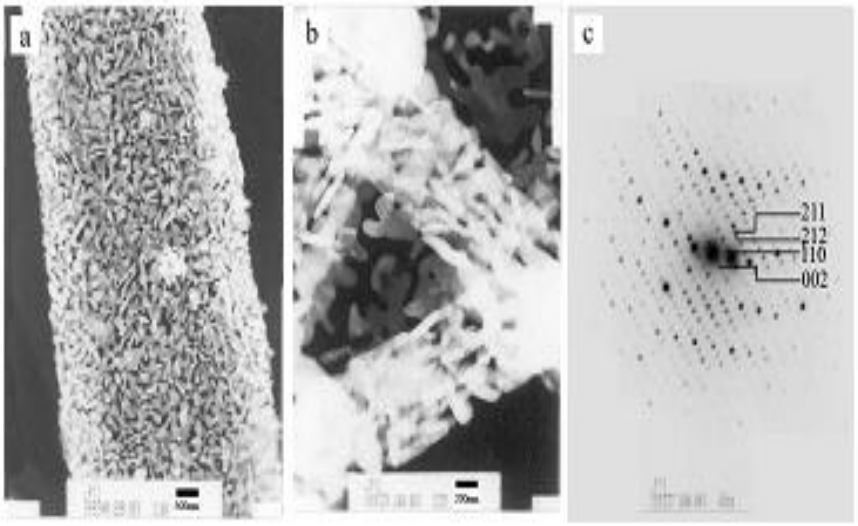

Fig. 6. TEM images(a, b) and SAED patterns(c) of $La_2Ti_2O_7$:5 %Eu^{3+} nanobelts annealed at 800 °C

3.4. Luminescence properties

Fig. 7 shows the excitation spectra of $La_2Ti_2O_7$: x mol%Eu^{3+}(x=1, 5, 7, 9) nanobelts monitored at 615 nm. In the excitation spectra, the wide band ranging from 260 to 360 nm is associated with the charge transfer(CT) transition of Eu^{3+}, while the other bands are assigned to the f-f electrons transitions of Eu^{3+}. The strongest peak locations of the CT band in samples (a) to (d) are around 270, 281, 285, and 287 nm, respectively. This implies that the CT band is red-shifted with the increase of doping Eu^{3+} ion concentration. It is well-known that the CT band is closely related to the covalency between O^{2-} and Eu^{3+} and the coordination environment around Eu^{3+}. Generally, the Eu^{3+}, the adjacent O^{2-}, and the sub-adjacent La^{3+} can form Eu^{3+}- O^{2-}-La^{3+} pairs and the electrons transfer from the 2p orbital of O^{2-} ions to the $4f^6$ orbital of Eu^{3+} to form the CT band. So, the energy for the migration of the p electrons depends on the potential field acting on the O^{2-} ions, which are derived from the surrounding ions. The red-shift of the CT band indicates that the potential field coming from the La^{3+} ions has less effect on the O^{2-}, in other words, less energy is needed to cause the electrons to transfer. At this time, the bond length between Eu^{3+} and O^{2-} becomes shorter and the mixture of wave function of Eu^{3+} and O^{2-} is enhanced.

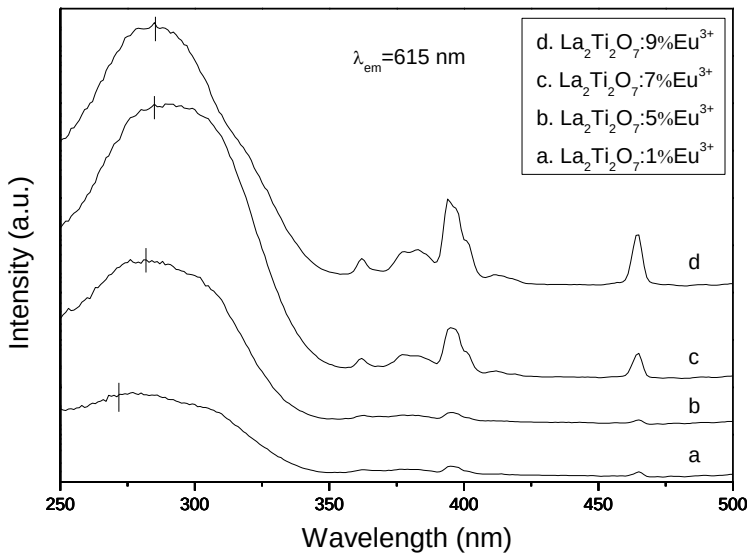

Fig. 7. Excitation spectra of $La_2Ti_2O_7$:x mol%Eu^{3+}(x=1, 5, 7, 9) nanobelts

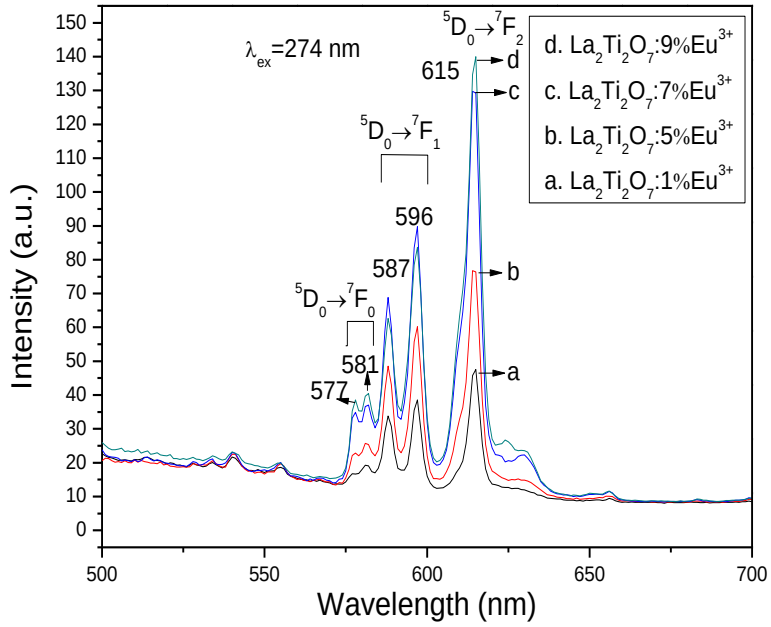

Fig. 8. Emission spectra of $La_2Ti_2O_7$:xmol%Eu^{3+}(x=1, 5, 7, 9) nanobelts (color online)

Fig. 9 shows the emission spectra of the $La_2Ti_2O_7$:x mol%Eu^{3+}(x=1, 5, 7, 9) nanobelts. Under the excitation of 274 nm, the nanobelts show similar emission peaks from 525 nm to 625 nm. The strongest emission peak at 615 nm can be assigned to the $^5D_0 \rightarrow {}^7F_2$ transitions of Eu^{3+} ions, while the peaks at 577 and 581 nm, 587 and 596 nm are ascribed to the $^5D_0 \rightarrow {}^7F_J$(J = 0, 1) transitions of Eu^{3+} ions. Other small peaks are attributed to TiO_6 octahedra centres [17] The layered perovskite $La_2Ti_2O_7$ structure contains four different crystallographic sites which can accommodate Eu^{3+} ions. Two of them possess C_1 point symmetry, which accommodate La^{3+} ions 9-fold coordination in layers. In the interlayer region, the La^{3+} ions are adapted in eight or seven-coordinated environments.[10] It is established that $^5D_0 \rightarrow {}^7F_2$ transition of Eu^{3+} ions, which is hypersensitive to the symmetry of coordinated environment, is usually forbidden in a crystalline environment with inversion symmetry. From the PL spectrum in Fig. 9, it is observed that the electric-dipole $^5D_0 \rightarrow {}^7F_2$ transition is stronger than that of the magnetic-dipole $^5D_0 \rightarrow {}^7F_1$ transition, suggesting that the position of Eu^{3+} have no inversion symmetry.

Fig. 9 shows the dependence of the PL emission intensity on Eu^{3+}doping concentration(x) in $La_2Ti_2O_7$:x mol % Eu^{3+}. It can be found that the PL emission intensity of Eu^{3+}increases with its doping concentration(x) from 1mol% to 9mol% without concentration quenching effect. This is probably due to the special layered structure of $La_2Ti_2O_7$ matrix [16, 22].

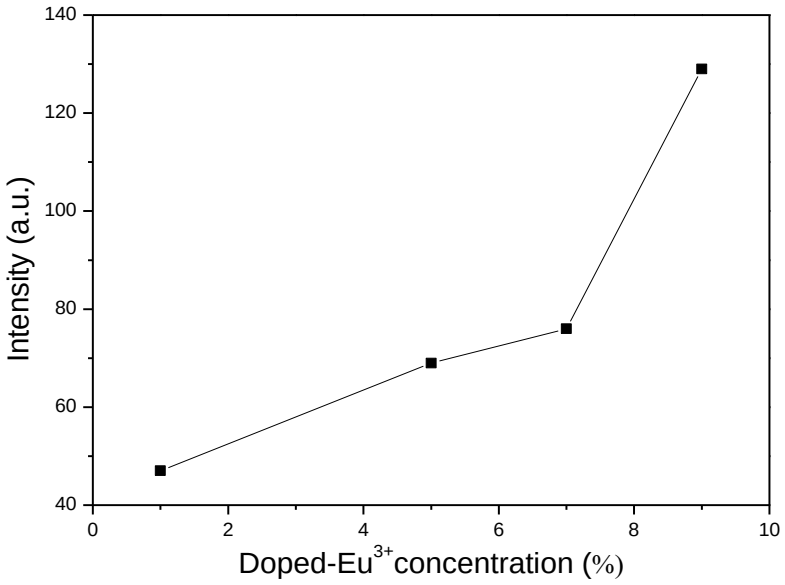

Fig. 9. Change of the emission peak intensity of 615 nm with different Eu^{3+} doping concentrations

3.5. Formation mechanism for the $La_2Ti_2O_7:Eu^{3+}$ nanobelts

The process of electrospinning is so complicated that the formation mechanism for nanobelts via electrospinning remains an open question [23, 24] On the basis of above analytic results, we propose the formation mechanism for $La_2Ti_2O_7:Eu^{3+}$ nanobelts, as shown in Fig. 10. The nanobelts was obtained by choosing the right kind of PVP, suitable solution viscosity and positive high voltage, the experimental parameters were provided in the manuscript. Because the viscosity of the spinning solution for preparing nanobelts was higher, and the applied voltage was lower, so that the spinning velocity was slower. The charge repulsion force had adequate time to stretch the jets into belt shape, led to the formation of composite nanobelts. The morphologies of the composite nanostructures were basically retained after performing the following calcination process. Rare Earth nitrate, $Ti(SO_4)_2$ and PVP were mixed with DMF to form sol with certain viscosity. PVP acted as template during the formation of $[La(NO_3)_3+Ti(SO_4)_2+Eu(NO_3)_3]$/PVP composite nanobelts. Cations and anions were mixed or absorbed onto PVP to form $[La(NO_3)_3+Ti(SO_4)_2+Eu(NO_3)_3]$/PVP composite nanobelts under electrospinning. During calcination process, DMF in the composite belts moved to the surface of the belts, and eventually was evaporated from the composite belts. With the increase in calcination temperature, PVP, $NO_3^-$and SO_4^{2-} were oxidized to volatilize, cations were oxidized into $La_2Ti_2O_7:Eu^{3+}$ crystallites, many crystallites were combined into small nanoparticles, then some small nanoparticles sintered into big nanorods, and these big nanorods were mutually connected to generate $La_2Ti_2O_7:Eu^{3+}$ nanobelts. It was found from experiments that content of PVP in the starting mixed sol had important impact on the formation of $La_2Ti_2O_7:Eu^{3+}$ nanobelts.

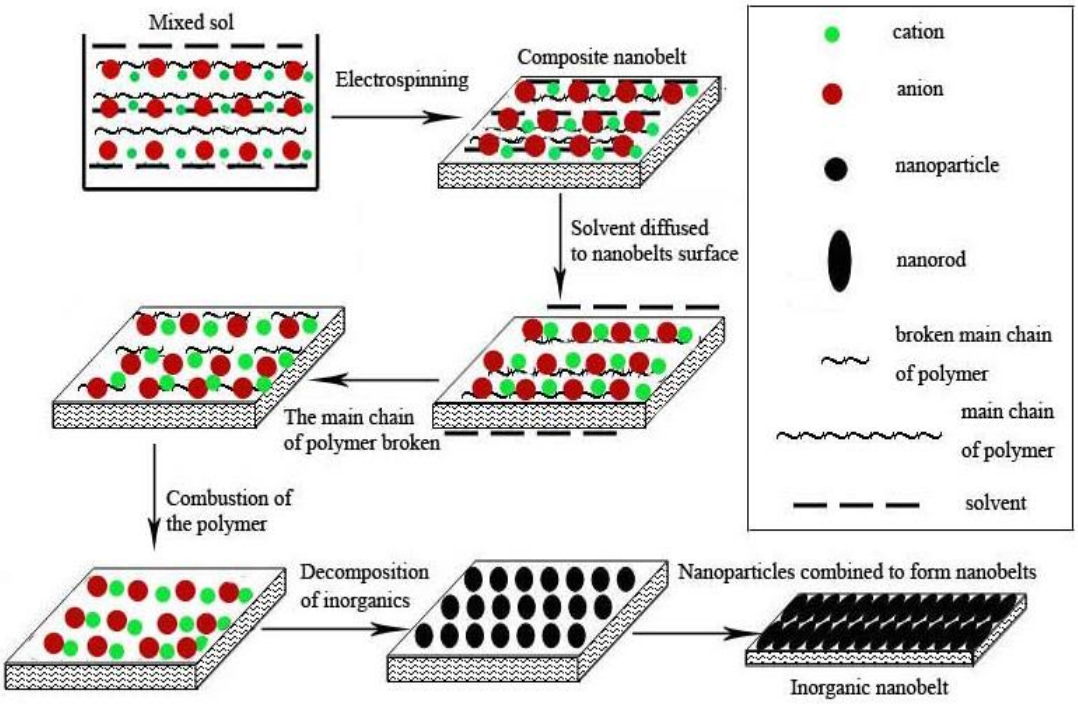

Fig. 10. Illustrative diagram of formation mechanism of $La_2Ti_2O_7:Eu^{3+}$ nanobelts (color online)

4. Conclusions

Quasi-one-dimensional $La_2Ti_2O_7$:x mol%Eu(x=1,5,7,9) nanobelts have been successfully synthesized by means of electrospinning technique combined sol-gel process. The $La_2Ti_2O_7:Eu^{3+}$ nanobelts are monoclinic in structure with space group $P2_1$, and the width and thickness of the nanoblets is 3 μm and 140 nm, respectively. $La_2Ti_2O_7:Eu^{3+}$ nanobelts are composed of nanorods with the length ranging from 270 to 660 nm. The luminescence analysis of the $La_2Ti_2O_7$: Eu^{3+} nanobelts indicates that the nanobelts emit the main emission peak at 615 nm, which could be applied in the field of optical telecommunication and optoelectronic devices.

Acknowledgments

This work was financially supported by the Scientific Development Program of Jilin Province (Grant No. YDZJ202201ZYTS376, 20170520152JH), and the Science and Technology Research Project of the Education Department of Jilin Province during the thirteenth five-year plan period (Grant No. JJKH20230328KJ, JJKH20180580KJ).

References

[1] H. Çolak, E. Karaköse, Mater. Sci. Semicond. Process **101**, 230 (2019).
[2] J. Cheng, Y. Jun, J. Qin, S. H. Lee, Biomaterials **114**, 121 (2017).
[3] P. Rathore, J. D. Schiffman, ACS Appl. Mater. Interfaces **13**, 48 (2021).
[4] Z. Y. Hou, C. X. Li, P. A. Ma, Z. Y. Cheng, X. J. Li, X. Zhang, Y. L. Dai, D. M. Yang, H. Z. Lian, J. Lin, Adv. Funct. Mater. **22**, 2713 (2012).
[5] Z. Y. Hou, G. G. Li, H. Z. Lian, J. Lin, J. Mater. Chem. **22**, 5254 (2012).
[6] Z. Y. Hou, C. X. Li, P. A. Ma, G. G. Li, Z. Y. Cheng, C. Peng, D. M. Yang, P. P. Yang, J. Lin, Adv. Funct. Mater. **21**, 2356 (2011).
[7] Z. Y. Hou, P. P. Yang, C. X. Li, L. L. Wang, H. Z. Lian, Z. W. Quan, J. Lin, Chem. Mater. **20**, 6686 (2008).
[8] D. Han, A. J. Steckl, ChemPlusChem. **84**, 1453 (2019).
[9] Y. Liu, Q. H. Zhang, W. B. Yuan, X. P. Fan, B. Du, P. Li, L. H. Xie, Food Sci. **42**, 1 (2020).
[10] E. Tavassoli, S. A. H. Goli, M. Fathi, Food Bioprocess Tech. **11**, 427 (2018).
[11] C. C. Li, H. C. Xiang, L. Fang, Ceram. Int. **42**, 11453 (2016).
[12] Y. Li, L. Jiang, Z. Jiao, D. Y. Liang, Q. Chen, J. G. Zhu, Phys. Status Solidi A **217**, 1900685 (2020).
[13] Y. Cao, P. Tang, Y. Han, W. Qiu, J. Alloy. Compd. **842**, 155581 (2020).
[14] M. Lu, Y, Cao, Y. Xue, W. Qiu, ACS Omega **6**, 27994 (2021).
[15] Y. Cao, P. Tang, W. Qiu, T Zhao, ACS Omega **5**, 29722 (2020).
[16] Y. Li, T. Lee, L. Jiang, J. Electron. Mater. **49**(4), 2584 (2020).
[17] X. Li, H. Cai, L. Ding, J. Alloy. Compd. **541**, 36 (2012).
[18] J. Y. Park, S. J. Park, M. Kwak, J. Lumin. **201**, 275 (2018).
[19] M. Erdem, S. B. Cantürk, G. Eryürek, Spectrochim. Acta A Mol. Biomol. Spectrosc. **270**, 120854 (2022).
[20] M. Gao, X. F. Lu, M. Q. Chi, S. H. Chen, C. Wang, Inorg. Chem. Front. **4**, 1862 (2017).
[21] M. Q. Chi, S. H. Chen, M. X. Zhong, C. Wang, X. F. Lu, Chem. Commun. **54**, 5827 (2018).
[22] L. B. Fan, Q. L. Ma, J. Tian, D. Li, X. Xi, X. T. Dong, W. S. Yu, J. X. Wang, G. X. Liu, J. Mater. Sci. **53**, 2290 (2018).
[23] W. Huang, Z. Tong, R. Wang, Ceram. Int. **46**, 26441 (2020).
[24] X. Q. Wu, Z. D. Shao, Q. Liu, J. Colloid Interf. Sci. **553**, 156 (2019).

*Corresponding author: bifei1224@163.com